Acta Oceanol. Sin., 2024, Vol. 43, No. 3, P. 15–29
https://doi.org/10.1007/s13131-023-2270-y
http://www.aosocean.com
E-mail: ocean2@hyxb.org.cn

Observing eddy dye patches induced by shear instabilities in the surf zone on a plane beach

Chunping Ren[1, 2*], Nannan Fu[1], Chong Yu[1], Yuchuan Bai[2], Kezhao Fang[3]

[1] State Key Laboratory of Hydraulic Engineering Simulation and Safety, Tianjin University, Tianjin 300072, China

[2] College of Water Resource Science and Engineering, Taiyuan University of Technology, Taiyuan 030024, China

[3] State Key Laboratory of Coastal and Offshore Engineering, Dalian University of Technology, Dalian 116024, China

Received 2 June 2023; accepted 20 October 2023

Abstract

The effects of surf zone eddy generated by alongshore currents on the deformation and transport of dye are still poorly understood, and related tracer release experiments are lacking. Therefore, a tracer release laboratory experiment was conducted under monochromatic, unidirectional incident waves with a large incident angle (30°) on a plane beach with a 1:100 slope in a large wave basin. A charge-coupled device suspended above the basin recorded the dye patch image. The evolution of eddy dye patch was observed and the transport and diffusion were analyzed based on the collected images. Subsequently, a linear instability numerical model was adopted to calculate the perturbation velocity field at the initial stage. The observation and image processing results show that surf zone eddy patches occurred and were separated from the original dye patches. Our numerical analysis results demonstrate that the structure of the perturbation velocity field is consistent with the experimental observations, and that the ejection of eddy patches shoreward or offshore may be ascribed to the double vortex.

Key words: surf zone, tracer release experiment, evolution of eddy patch, shear instability of alongshore currents

Citation: Ren Chunping, Fu Nannan, Yu Chong, Bai Yuchuan, Fang Kezhao. 2024. Observing eddy dye patches induced by shear instabilities in the surf zone on a plane beach. Acta Oceanologica Sinica, 43(3): 15–29, doi: 10.1007/s13131-023-2270-y

1 Introduction

The surf zone extends from the breaker zone to the shore and to the seaward extent of depth-limited breaking, characterized dynamically by the importance of eddies and wave-driven flows. At the shoreline, pollutants can enter through storm overflow discharges from overloaded combined and separate sewerage systems during rainfall events, thus making the surf zone crucial for nearshore ecosystems. Alongshore currents (Feddersen, 1998; Longuet-Higgins, 1970; Tang et al., 2016) are induced under obliquely incident wave conditions in the surf zone when wave breaking occurs. Simultaneously, turbulence (Feddersen, 2012) is generated, so the water column (Hally-Rosendahl et al., 2014) is vertically mixed. Field observations and modeling indicate that surf zone eddies (Clark et al., 2010, 2011; Spydell and Feddersen, 2012a) significantly affect the dispersion and dilution of surf zone pollutants (Clark et al., 2010, 2011; Spydell and Feddersen, 2012a, b) and material transport (e.g., of larvae and nutrients) between the surf zone and inner shelf (Brown et al., 2015; Hally-Rosendahl and Feddersen, 2016; O'Dea et al., 2021; Wu et al., 2020). The generation mechanism of surf zone eddies includes intrinsic shear instability (Noyes et al., 2004; Oltman-Shay et al., 1989) and extrinsic wave forcing (short crested (Feddersen, 2014; Peregrine, 1998) or wave groups (Long and Özkan-Haller, 2009; Reniers et al., 2004)). It was suggested that shear instability might dominate surfzone eddy generation for highly narrowbanded frequency and direction and obliquely large incident waves (Feddersen, 2014). However, the eddies' evolution of surf zone tracers is poorly understood.

According to linear stability theory, background vorticity $(\partial V/\partial x)/h$ (V is mean alongshore current velocity; x is the distance from the shoreline; h is water depth) arises from the longshore current's shear. This vorticity response acts as a restoring force for the perturbation. Thus, this is an intrinsic eddy generation mechanism. The instabilities of alongshore currents have been observed in field observations (Oltman-Shay et al., 1989) and laboratories (Ren et al., 2012), both numerically (Allen et al., 1996; Noyes et al., 2005; Özkan-Haller and Kirby, 1999; Slinn et al., 1998) and analytically (Feddersen, 1998). Shear instability motion was first observed in the field by Oltman-Shay et al. (1989), with fluctuation periods of 50–500 s alongshore at 40–250 m wavelengths. Elsewhere, Bowen and Holman (1989) formulated the theoretical basis for the instability of the alongshore current. They argued that it arises mainly from the cross-shore velocity gradient of the mean alongshore current, essentially an intrinsic eddy generation mechanism. Subsequent field experiments (Noyes et al., 2004) showed that shear waves are generated primarily in the highly sheared region, just seaward of the location of the maximum mean alongshore current velocity. Also, strong shear instability can be observed in the laboratory on the plane slope with gradients 1:40 and 1:100 under monochromatic, unidirectional, and obliquely incident waves with a large incident angle (30°) (Ren et al., 2012). However, the authors did not of-

Foundation item: The open foundation of the State Key Laboratory of Hydraulic Engineering Simulation and Safety under contract No. HESS-2006; the Shanxi Province Science Foundation under contract No. 202103021224116; the research project supported by Shanxi Scholarship Council of China under contract No. 2023-067.

*Corresponding author, E-mail: chunpingren@163.com

fer a detailed discussion of the evolution and spatial characteristics of separated eddy dye patches induced by shear instabilities.

Although Feddersen (2014) suggested that surfzone eddies (vorticity) are generated through the extrinsic mechanism of breaking wave vorticity forcing, with a 10–100 m range alongshore, the modeling snapshot result at t = 91.2 min showed that simulated tracer patch meanders 0–100 m alongshore, utterly different with downstream dye patches (http://falk.ucsd.edu/funwaveC.html, HB06 dye releases example). This deduction may be attributed to the instability of alongshore currents and the suppression of surf zone cross-shore mixing by the currents (Spydell, 2016).

According to the extrinsic wave-breaking mechanism in generating surf zone eddies, the eddies coalesce to form transient rip currents. The episodic offshore directed flows eject surf zone water onto the inner shelf (Johnson and Pattiaratchi, 2004). Further, the material exchange between the surf zone and inner shelf associated with transient rip currents has been studied using a numerical method and field observations (Grimes et al., 2020a, 2020b, 2021; Hally-Rosendahl et al., 2014, 2015; Moulton et al., 2021; O'Dea et al., 2021). Therefore, these surf zone eddies are critical to the material exchange, and exploring the generation forced by shear instabilities is necessary.

Shoreline dye release experiments in fields have been conducted to quantify the surf zone tracer transport and exchange between the surf zone and inner shelf (Clark et al., 2010; Grimes et al., 2021; Hally-Rosendahl et al., 2014, 2015). Whether these release experiments were continuous or instantaneous, long or short alongshore, these observations show that the maximum tracer concentration occurs roughly periodically alongshore from the release location to the tracer front position. Correspondingly, the tracer head in the cross-shore direction is rhythmic in the surf zone and on the inner shelf.

Alongshore meandering (spreading) tracer patches are commonly ascribed to shear instability or dispersion. According to linear stability theory, the generated shear waves have phase velocities, lengths, and time scales in the alongshore direction. The extrinsic wave-breaking mechanism in generating surfzone eddies cannot sufficiently describe these alongshore current oscillations (Noyes et al., 2005; Oltman-Shay et al., 1989; Ren et al., 2012). However, after dye release, a prolonged surf-zone concentration decay $\widetilde{y} \approx 500$ m was observed (Hally-Rosendahl et al., 2014). Rip currents on beaches with longshore-uniform bathymetry are often transient and lack preferred alongshore locations. Therefore, it is likely due to the recirculation of inner-shelf dye or weak eddy ejection dominated by shear instability. The lack of quantitative field measurements of tracer evolution at these time/space scales has prevented a detailed assessment of this mechanism. Therefore, precise measurements may be needed to assess the intrinsic eddy generation mechanism.

When the alongshore wave-guide current is generated (due to the shear of the alongshore current in the cross-shore direction), it is yet unverified whether the turbulence caused by the wave breaking is also affected by the shear of the current. This concept has not been studied using models that consider shear instability and wave breaking. For weak alongshore currents or V = 0, the vertical change of the currents in the surf zone is enhanced, resulting in the vertical shear of current enhancements. According to shear instability theory, as long as there is a flow shear, the background vorticity can be generated, driving the generation of these eddies. Therefore, the surf zone vortex observed in the case of a weak current is also very likely to be driven by the current shear force and gradually evolve into a large-scale vortex.

Regarding these eddies caused by the shear instability of the alongshore current, the corresponding tracer experiment and the impact on the propagation and diffusion of pollutants inside and outside the surf zone need further study. The use of pollutants or floats for field or laboratory experiments can efficiently investigate the mixing (Abolfathi and Pearson, 2017; Abolfathi et al., 2020), the propagation of pollutants and eddy generation mechanism in the surf zone, observe the characteristics of the vortex in the surf zone, and verify the mathematical model (Abolfathi and Pearson, 2014; Clark et al., 2011; Grimes et al., 2021; Pearson et al., 2009). The surf zone tracer diffusion and dispersion can be studied by measuring the concentration distribution on the cross-section (Clark et al., 2010), remote sensing (Grimes et al., 2021), radar (O'Dea et al., 2021), and laboratory image (Abolfathi and Pearson, 2014). The first three are more suitable for large-scale analysis in the field, but the accuracy is relatively low. Laboratory image acquisition has advantages in terms of accuracy, and the subtle processes of propagation, diffusion, and vortex generation in the surf zone can be obtained in a smaller area. Instantaneous or continuous release of pollutants in the surf zone has been used to study the propagation and diffusion of pollution inside and outside the surf zone. Still, none of these studies revealed the effect of shear instability on the propagation and diffusion process of pollutants around or within the surf zone.

Therefore, based on the surf zone tracer laboratory experiment, we studied the characteristics of surf zone eddies and propagation driven by the instability of the alongshore current. The paper also verifies whether the fluctuation of the alongshore current can produce eddies in the surf zone on the alongshore uniform slope under monochromatic, unidirectional, and obliquely incident waves with a large incident angle. The research results may provide an implication for understanding surf zone eddy generated by shear instabilities of alongshore currents.

This paper analyzes laboratory surf zone tracer observations on a plane beach to investigate the behavior of plumes generated by the shear instabilities of alongshore currents. Section 2 describes the laboratory experiment, while Section 3 describes the evolution of the eddy patch. The extension and transport of these eddy patches are estimated by tracking. Section 4 reports the shear instability analysis of four cases. Some study limitations, including experimental and numerical analyses are discussed in Section 5. The conclusions are summarized in Section 6.

2 Methods

2.1 *Experimental setup*

To observe the surf zone eddy generated by the instabilities of alongshore currents, we conducted an alongshore current and dye release experiment in the laboratory on the plane beach with slope 1:100 under monochromatic, unidirectional, and obliquely incident waves with a 30° incident angle. The 1:100 slope was chosen to induce a wider surf zone and variations in longshore current velocity gradients (i.e., significant front shear and backshear) in the surf zone, which increases the shear instability. Laboratory experiments on the shear instability of longshore currents have been carried out. For instance, Visser (1991) experimented on alongshore currents on plane slopes 1:10 and 1:20. Still, previous experimental results did not indicate the temporal variations of alongshore currents. Measurements of the unstable motion of alongshore currents suggested that instability occurs on a barred beach but not on a non-barred beach (Reniers et al., 1997). Although they observed oscillations for regular and random waves on a barred beach, Reniers et al. (1997) suggested

that such observations do not necessarily preclude shear instability on a plane beach. Elsewhere, the lack of detection of shear waves in laboratory experiments has been attributed to the limited length of the wave basin and the damping effect of bottom friction (Putrevu and Svendsen, 1992), (i.e., the viscous damping probably suppresses the shear instability in laboratory experiments). The observations are described elsewhere (Ren et al., 2012) and briefly introduced here. The experiment was carried out in the 55 m × 34 m × 1.0 m wave basin at the State Key Laboratory of Coastal and Offshore Engineering, Dalian University of Technology. The beach makes an angle of 30° to the wave generator, creating a large incident angle and a long beach that allows more room for alongshore current instability to develop. Two concrete plane profiles with 1:40 and 1:100 slopes were constructed (Fig. 1).

The present study analyzed only the measurement results for the 1:100 slope because the surf zone width is sufficient to detect the shear instabilities as much as possible. Putrevu and Svendsen (1992) mentioned that it is appropriate to consider spatial scales corresponding to this topography when discussing possible shear wave instabilities in laboratory measurements. Another reason is that enough horizontal spatial scale can be provided to transport the dye patch, particularly eddy patch separation. Also, it was demonstrated that the entire process of eddy dye patch formation on the 1:100 slope can be observed, not on the 1:40 slope (according to the present observation). The coordinate system used has x as the cross-shore coordinate that increases offshore with the still water line $x = 0$ m, and y as the alongshore coordinate. The still-water depth over the horizontal bottom was 0.45 m for the 1:40 slope experiments and 0.18 m for the 1:100 slope experiments. A wave generator consisting of individual wave paddles was located at the offshore end of the basin, having a total length of 24.5 m. The paddles were moved in phases. Monochromatic, random, unidirectional, and obliquely incident waves were generated in the experiments. Irregular waves were generated using a JONSWAP spectrum with a peak enhancement factor γ of 2.5. To make alongshore currents recirculate within the wave basin and produce uniform movements, a circulation channel with a 3.0 m width at the two lateral ends and a 1.0 m depth (the same as in the horizontal bottom part of the basin) was introduced around the beach.

A total of 32 two-dimensional velocity meters (VMs) in two identical arrays of 16 (Fig. 1) measured the flow field at a 20 Hz sampling rate. These VMs were set at one-third of the water depth from the bottom, approximately the depth at which depth-averaged alongshore currents occurred. The distance of the VMs from the shoreline for the slope 1:100, x, is given in Table 1. The strain-type velocity meters used were suitable for long-period horizontal oscillations (>2 s) and for measuring long-period unstable alongshore currents in the present study.

Steady and strong alongshore currents can be generated (Ren et al., 2012). Here, four wave conditions (Table 2) were chosen to analyze the surf zone tracer evolution. The surf-zone width and the offshore values $\xi_0 = \tan(\beta)/\sqrt{H_0/L_0}$ and H_0/L_0 (where $\tan(\beta)$ is the beach slope; H_0 and L_0 are the wave height and wave length at the wave maker, respectively) are also given according to wave height variations corresponding to these four cases (Ren et al., 2012). ξ_0 is the Iribarren number which characterizes the breaker type. The ξ_0 values for the four cases were less than 0.4, indicating that the spilling breaking occurred in the present experiment. In addition, the monochromatic wave conditions with varying wave steepness ($H_0/L_0 = 1 - 2\%$) represented the wave conditions on gentle beaches.

2.2 *Dye release*

A dye release experiment was conducted to observe the oscillation motions visually and spatially as the longshore currents were generated. The dye (ink, in this case) was continuously released in the surf zone using a long, 0.8 cm-diameter thin tube. The dye-release point was located at $x \approx 4.5$ m, $y \approx 3$ m for the 1:100 slope, and approximately one-third of the water depth from the bottom. A charge-coupled device (CCD) suspended 11.6 m above the basin recorded the dye patch image (Fig. 2).

The pixels of the image were 752 × 576, corresponding to 5 m × 7 m (denoting cross-shore and alongshore dimensions, respectively). Figure 2 illustrates the image-collecting system. When the alongshore current was stable (based on the time histories of the current meter), the ink was released continuously into the surf

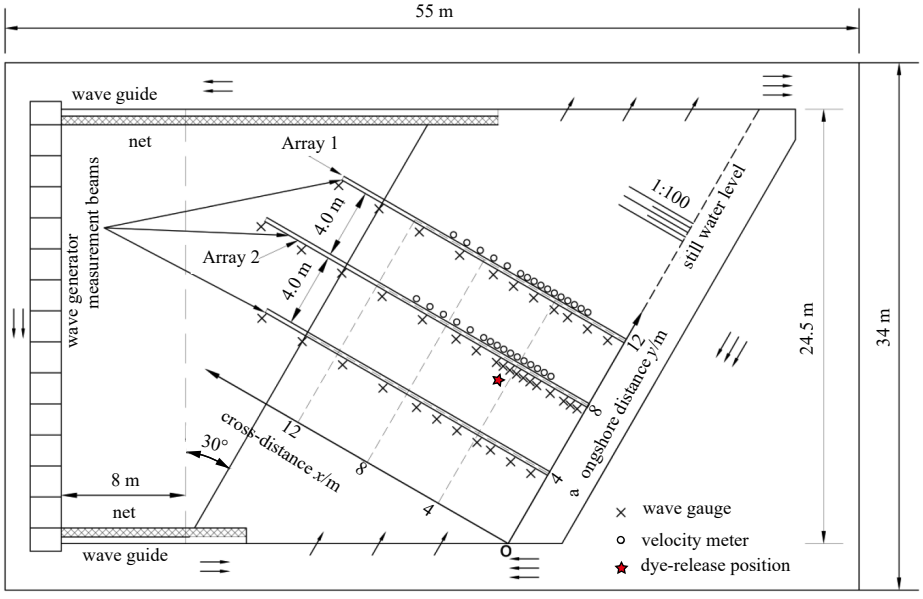

Fig. 1. Experimental layout.

Table 1. The distances (x) of velocity meters (VMs) from the shoreline

VM	x/m	VM	x/m
1	2.0	9	6.0
2	2.5	10	6.5
3	3.0	11	7.0
4	3.5	12	8.0
5	4.0	13	9.0
6	4.5	14	10.0
7	5.0	15	11.0
8	5.5	16	12.0

Table 2. Test conditions

Case	Incident wave	Slope	D/cm	H/cm	T/s	x_b/m	L_0	ξ_0	H_0/L_0
1	regular waves	1:100	18	2.7	1.5	5.2	3.51	0.11	0.01
2	irregular waves	1:100	18	2.4	1.0	6.2	1.56	0.08	0.02
3	irregular waves	1:100	18	3.9	1.0	9.8	1.56	0.06	0.02
4	irregular waves	1:100	18	5.0	1.5	10.2	3.51	0.08	0.01

Note: D, still water depth; H, mean wave height; T, peak period; L_0 and H_0, wave length and wave height at the wave maker, respectively; x_b, surf-zone width.

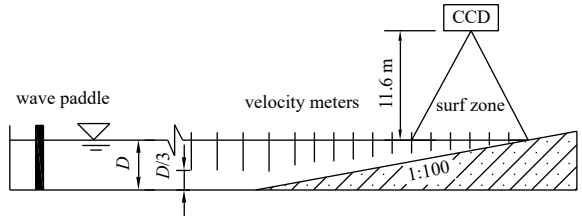

Fig. 2. An illustration of collecting dye patch images using charge-coupled device (CCD).

zone simulated by a continuous source. The ink was pulled to the vicinity of the surf zone through a thin tube when released with about 50 cm^3/s flow. The CCD system sampled the dye patch movement approximately every 1.0 s until the front part of the dye patch exited the CCD acquisition range under each wave condition.

The CCD system collects images with stricter requirements for the brightness of the environment. To collect clear images and coordinate transforms (transforms between world and image coordinates), the beach was made of white cement, forming a white background, and drawn 1 m × 1 m black mesh on the beach, making it easy to accurately analyze the characteristics of the ink patch in the surf zone.

Through experimental analysis, we found that visible eddy or alongshore meandering patches occurred in the four test cases. The parameters are given in Table 1.

2.3 *Image analysis procedure*

The image analysis procedure includes three steps. First, we extracted the dye patch boundaries using the Matlab image processing toolbox. In detail, this step involves subtracting the background image (collected before dye release) from the dye patch image (collected at some time during the dye release experiment), extracting the dye patch boundaries using Matlab image processing toolbox, such as colormap( ), im2bw( ), imclose( ) and so on. Thus, the dye patch boundaries can be obtained with coordinate transform. The second step is coordinate transform. To quantitatively analyze scales and the transport of surf zone dye patches, one necessary requirement for quantifying the information in a dye patch image is knowing the photogrammetric transformation between world and image coordinates. Here, we adopted the coordinate transformation method developed by Holland et al. (1997). These transforms require the world coordinate and the corresponding image coordinate as inputs. The 36 ground control points are used to transform between pixel and world coordinates (Fig. 3). The plane beach in this experiment was painted white, and square grids (1 m × 1 m denotes by two-arrow in Fig. 4 were drawn on the surface to transform from a pixel coordinate into a physical coordinate of identifiable ground control points. Figure 4 shows the image at t = 40 s for Case 1 (left), and the dye patch boundary transformed from pixel coordinate into the physical coordinate. At last, we focus on the eddy dye patches (solid blue rectangular box in Fig. 9), used to quantitatively analyze the diffusion and transport of the eddy patch with time.

3 Results

3.1 *Alongshore currents*

Figure 5 shows the recorded time series of cross-shore and alongshore current velocities for Case 1 (regular waves) at x = 4.5 m in the first velocity meter array. Large-amplitude and long-period oscillations occurred in the alongshore and cross-shore velocity components, also observed under all four conditions, with a 50 s period. The maximum alongshore current velocity (0.18 m/s) present at t = 115 s, and the mean over 40 s (the alongshore currents were gradually strong) to 180 s was approximately 0.12 m/s (Fig. 5b). The cross-shore velocity oscillated between 0.08 m/s

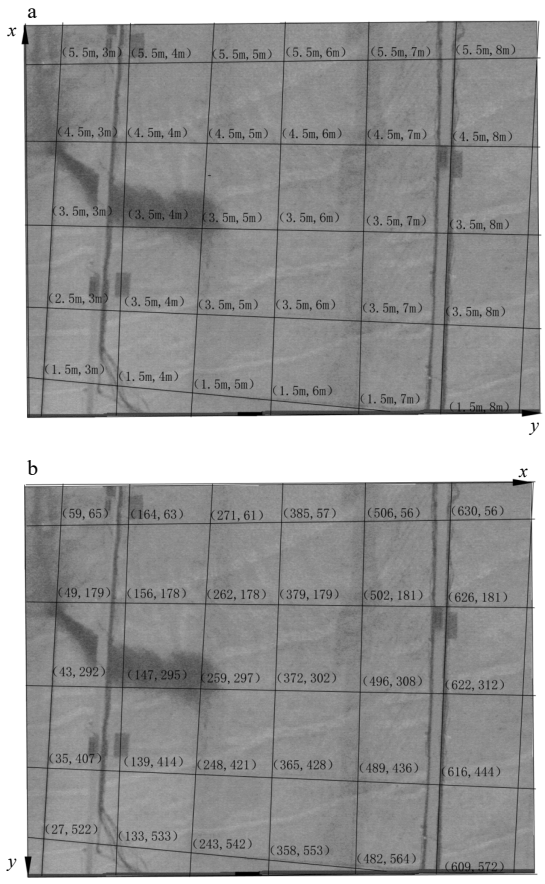

Fig. 3. The used ground control points in world coordinate (a) and pixel coordinate (b).

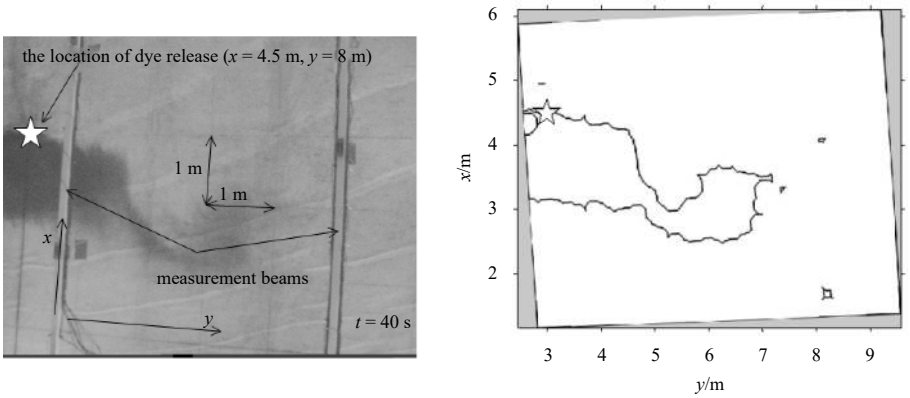

Fig. 4. Collected image at t = 40 s for Case 1 (left) and the dye patch boundary transformed from pixel coordinate into the physical coordinate (right). Star indicates the location of release.

and –0.08 m/s (Fig. 5a). To show the far infragravity motions clearly, low-pass finite impulse response filter was then applied to the data with threshold frequencies of 0.02 Hz for irregular waves and 0.04 Hz for regular waves (Fig. 5).

Ren et al. (2012) compared the cross-shore profiles of the mean alongshore velocities for the two velocity meter arrays, demonstrating that the generated mean alongshore currents were approximately uniform. Figure 6 shows the alongshore currents for Cases 1–4 (in meters) deployed in the second velocity meter array close to the dye release location. Each test was repeated thrice throughout the experiment to obtain compelling results; therefore, every cross-shore location had three values (some data were broken).

The longshore current profiles for the four cases (Fig. 6) were computed from the depth-averaged longshore momentum balance (Reniers and Battjes, 1997). The solid curves fitted to the longshore currents velocity measurement are also given. By comparison, we observed that the model results did not match the fitted data adequately, particularly at the shoreward side (frontshear) or seaward side (backshear) of the velocity profile (Baquerizo et al., 2001). Such is attributable to the model parameters. Nevertheless, the fitted results agreed more with the measurements. Based on linear instability theory, the instability mode is sensitive to the mean longshore current profile (Baquerizo et al., 2001). Therefore, the solid curves fitted to the results were used as input data for the linear instability analysis in Section 4. The maximum mean alongshore currents ($V_{\max}$) measurements varied between 0.09 m/s and 0.19 m/s for the four case examples. For Froude criterion of gravitational similarity, assuming field significant wave height H_s = 1.0 m, for Case 2 H_s = 0.027 m and $V_{\max}$ = 0.09 m/s, therefore, the length scale ratio λ_L = 37.04 and the velocity scale ratio $\lambda_V = \frac{V_{P,\max}}{V_{M,\max}} = \lambda_L^{0.5}$ (where $V_{P,\max}$ is the prototype value and $V_{M,\max}$ is the experiment result). Thus, the calculated field maximum of mean alongshore currents $V_{P,\max}$ corresponding to $V_{M,\max}$ for Case 2 is approximately 0.55 m/s. Therefore, we deduced that the mean alongshore currents generated in the present experiment are strong.

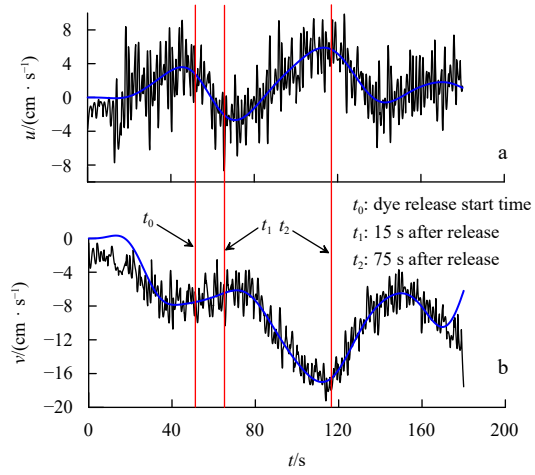

Fig. 5. Time series of cross-shore velocity u (a) and alongshore velocity v for Case 1 at the ink injection location (x = 4.5 m) (b). Solid blue line denotes the filtered results; three red lines indicate the dye release start time and 15 s and 75 s after release, respectively.

3.2 *Surf zone eddy generation process*

By observing the tracer images collected in the experiment, we found that surf zone eddies appeared under all four test conditions, and these tracer eddies gradually developed over time. During this process, these dye patches were meandering in the alongshore direction, similar to the HB06 modeling result at t = 91.2 min downstream of dye release from 0 m to 100 m (http://falk.ucsd.edu/funwaveC.html, HB06 dye releases example), with eddy ejection likely occurring at some moment.

Figure 7 shows the collected images of the dye patch at t = 15 s, 25 s, 35 s, 45 s, 55 s, 65 s, 75 s, 85 s, 95 s, and 105 s for Case 1 in the surf zone. Here, the detailed process of surf zone eddy generation was apparent. At the initial stage t = 15 s (corresponding to t_1 indicated using red line in Fig. 5, 15 s since ink release), the alongshore current velocity was about 0.08 m/s, and the ink patch was only transported in cross-shore direction, indicating that the stokes drift at the release position was larger than the alongshore current velocities. When the dye patch was transported onshore at some location, the dye patch gradually moved in alongshore direction due to the considerable increase of alongshore current at this location. Simultaneously, curl deformation occurred because the shear force $\partial V/\partial x$ increased with the mean alongshore current, resulting in vorticity forcing induced by alongshore current shear. For example, at t = 75 s (after release, corresponding to t_2 in Fig. 5, indicated using red line), the alongshore current was approximately 0.16 m/s, enough to drive the dye patch to move in the alongshore direction (the dye patch surrounded by the solid red rectangular box in Fig. 7g). At this

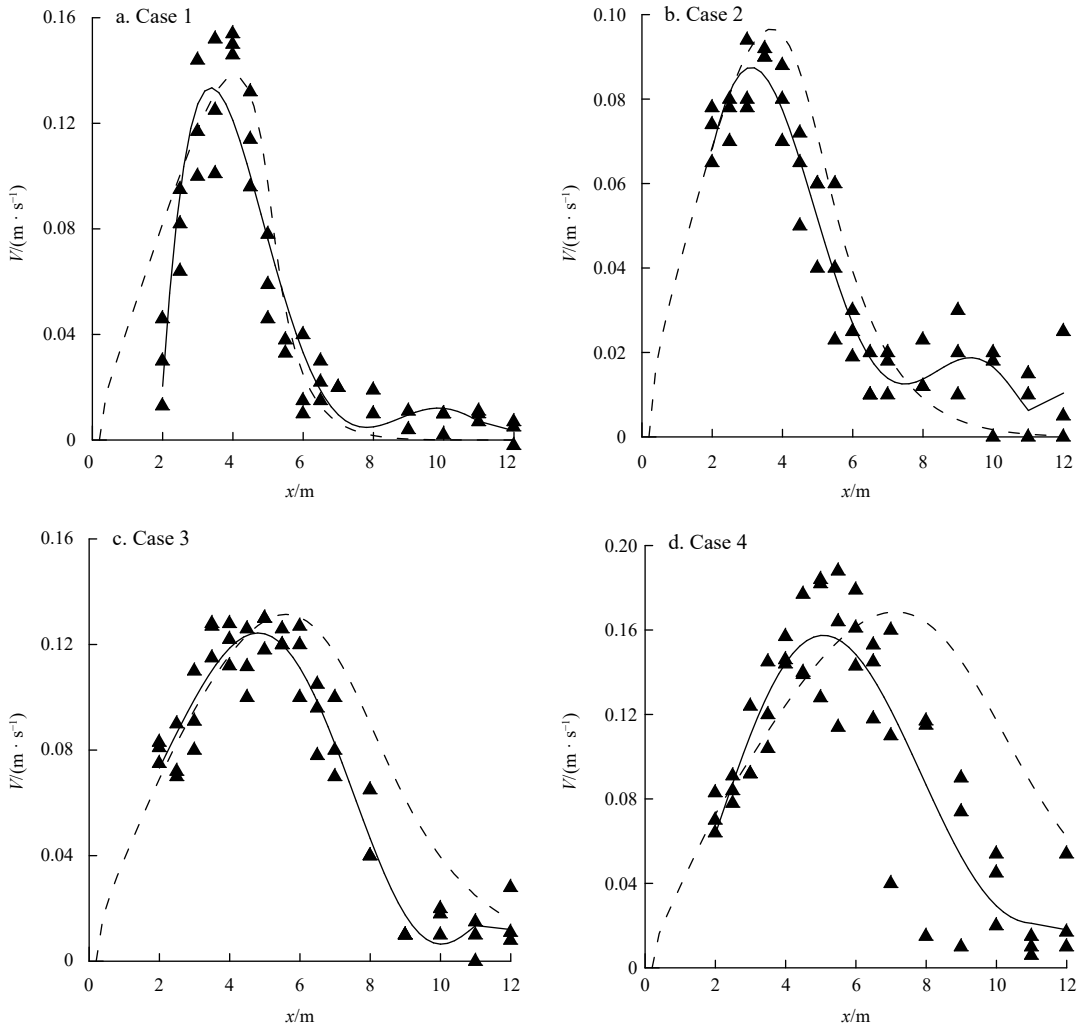

Fig. 6. Mean longshore current velocities for Cases 1–4. ▲, data; —, fitted curve; – – numerical simulation result.

time, relatively complete eddy was generated (the surrounding part of the dashed red rectangular box in Fig. 7g) and confined to the inner surf zone. This phenomenon may be induced by shear instability or background vorticity. With time, the eddy patch moved alongshore, not merging with the main part until it was transported out of the observation area. This occurrence suggests that the shear instability in strong alongshore currents persistently drove the dye patch.

In Fig. 8, the collected images for Cases 2–4 under regular incident waves are shown to examine the effects of wave conditions on the deformation pattern of the dye patch. We observed that these dye patches moved meanderingly in Case 2. Significant deformation of these dye patches occurred, and the front part of the dye patch formed an eddy shape. It was ejected offshore and shoreward for Cases 3 and 4, respectively (the solid red rectangular box in Figs 7b and c). In detail, these eddy shape patches for Case 4 were presented more sufficiently and completely than for Case 3. For Case 2, eddy shape patches were not observed, maybe due to the limited collection area. It means that the deformation may occur at some location downstream or in the observation area after a long release time. The above observation for Cases 1–4 demonstrated two types of deformation: meandering and eddy shape. More importantly, the two deformations were continuous; therefore, a persistent driving force was required.

As mentioned in Section 3.1, alongshore currents were strong for the four cases, and the alongshore current shear may be large enough to induce shear instability. Therefore, it suggests that the deformations of these dye patches were dominated by shear instability. For Cases 3 and 4, surf zone eddy shape patches appeared in the offshore and the onshore direction, respectively, indicating that the eddy induced by shear instability may eject shoreward or offshore. The ejection offshore was similar to transient rip currents, characterized by concentrated and ephemeral offshore flows that trap and advect surfzone tracers onto the innershelf, resulting in an alongshore patchy innershelf tracer field (Grimes et al., 2021; Hally-Rosendahl et al., 2014). Based on the previous study, transient rip currents are generated randomly on uniform beaches (Hally-Rosendahl et al., 2015). However, the perturbation velocity field induced by shear instability was periodic in the alongshore direction. That means surf zone eddies generated by shear instability are not random. At least, the meandering dye patch formation cannot be explained using the transient rip current generation mechanism.

3.3 *Horizontal diffusion and transport of eddy patches in cross-shore and alongshore direction*

These surf zone eddies significantly impact the diffusion and transport of dye patches in the cross-shore and alongshore direction. Here, quantitative analysis of the diffusion and transport

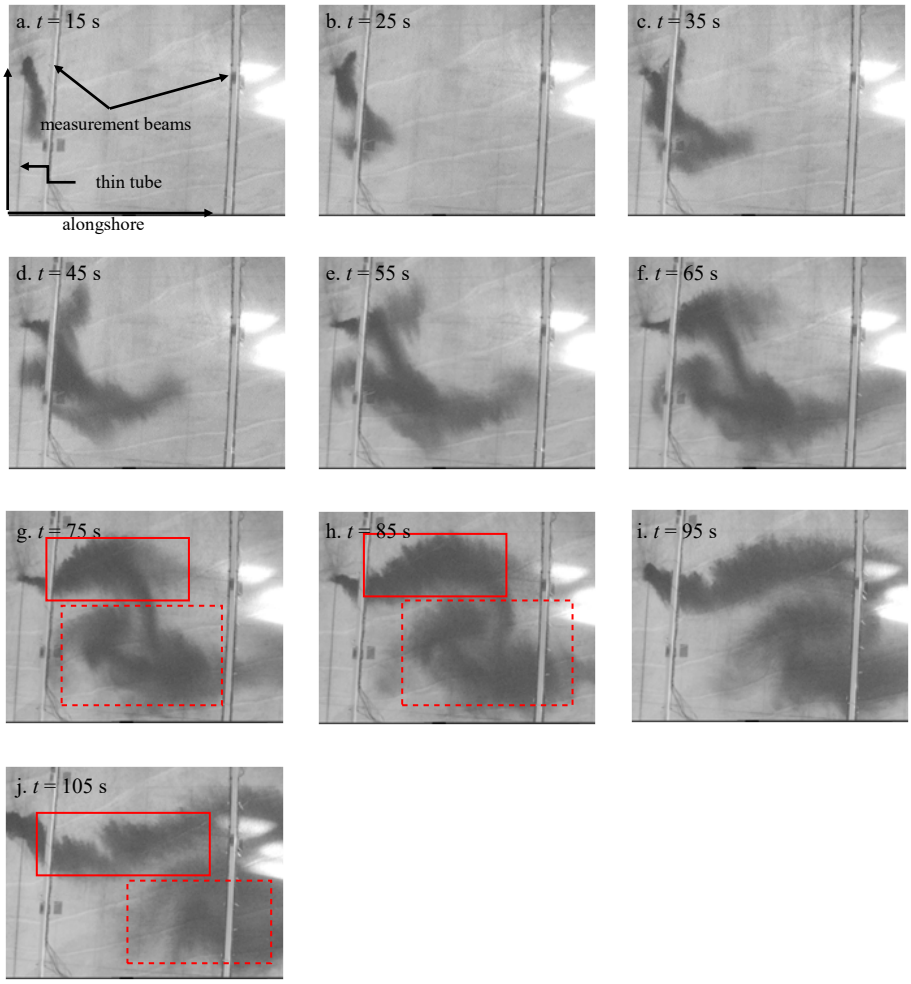

Fig. 7. Deformation of dye patch at t = 15 s, 25 s, 35 s, 45 s, 55 s, 65 s, 75 s, 85 s, 95 s, and 105 s for Case 1. The solid red and dashed rectangular boxes indicate the dye patches driven by alongshore currents and vorticity respectively.

was conducted by tracking the deformation and displacement of the approximate centroid of the eddy patch (the solid blue rectangular box in Fig. 9) with time.

First, these collected images were processed to obtain their boundaries at which the concentration was regarded as approximately 5% of the maximum (Figs 3 and 8). Next, we examined the diffusion and transport of eddy patches.

Here, diffusion velocities (V_{Dx}, V_{Dy}) and transport velocities (V_{Tx}, V_{Ty}) were used to assess the extension and transport of eddy patches for the four cases. Note that diffusion here refers to the extension of the boundary of the dye patch in the horizontal direction and is not determined by the traditional method for diffusion characteristics through concentration contours. This approach is mainly because this present study focuses on the observations and effects of unstable alongshore currents on pollutants. In Fig. 10, related parameters are given: (L_{x1}, L_{x2}) and (L_{y1}, L_{y2}) are the cross-shore and alongshore length scales at two different moments, respectively. Therefore, (V_{Dx}, V_{Dy}) and (V_{Tx}, V_{Ty}) are defined as follows:

$$V_{Dx} = \frac{\Delta L_x}{\Delta t}, \tag{1}$$

$$V_{Dy} = \frac{\Delta L_y}{\Delta t}, \tag{2}$$

$$V_{Tx} = \frac{\Delta S_x}{\Delta t}, \tag{3}$$

$$V_{Ty} = \frac{\Delta S_y}{\Delta t}, \tag{4}$$

where $\Delta L_x = L_{x2} - L_{x1}$, $\Delta L_y = L_{y2} - L_{y1}$; Δt is the time interval; $\Delta S_x = x_{c2} - x_{c1}$, $\Delta S_y = y_{c2} - y_{c1}$; $x_{c1} = x_1 - \frac{L_{x1}}{2}$, $x_{c2} = x_2 - \frac{L_{x2}}{2}$; $y_{c1} = y_1 - \frac{L_{y1}}{2}$, $y_{c2} = y_2 - \frac{L_{y2}}{2}$.

Based on the definition of diffusion and transport velocity given, ΔL_x, ΔL_y, Δs_x, and Δs_y were calculated by tracking the boundaries of every image in two directions at different times. This data was then fitted linearly (V_{Dx}, V_{Dy}) and (V_{Tx}, V_{Ty}) were estimated from the linear fit's slopes. Note that every collected dye patch under Case 2 was analyzed as a whole because separated eddy patches were not visibly observed; the eddy patches were analyzed under Cases 1, 3, and 4.

Figures 11–14 show the fitted results for Cases 1–4. In general, these correlation coefficients between the linear-fitted results and the measurement results are high. In addition to the V_{Dy} for Case 2 (Fig. 12b) and the V_{Tx} for Case 3 (Fig. 13c), the two correlation coefficients are very low. First, we noted that the ΔL_y and x_c vary in the smaller range of 0.4–0.3 m in Fig. 12b (Case 2) and Fig. 13c (Case 3), respectively. It suggested that the eddy dye patches for Case 2 were weakly diffused alongshore and barely

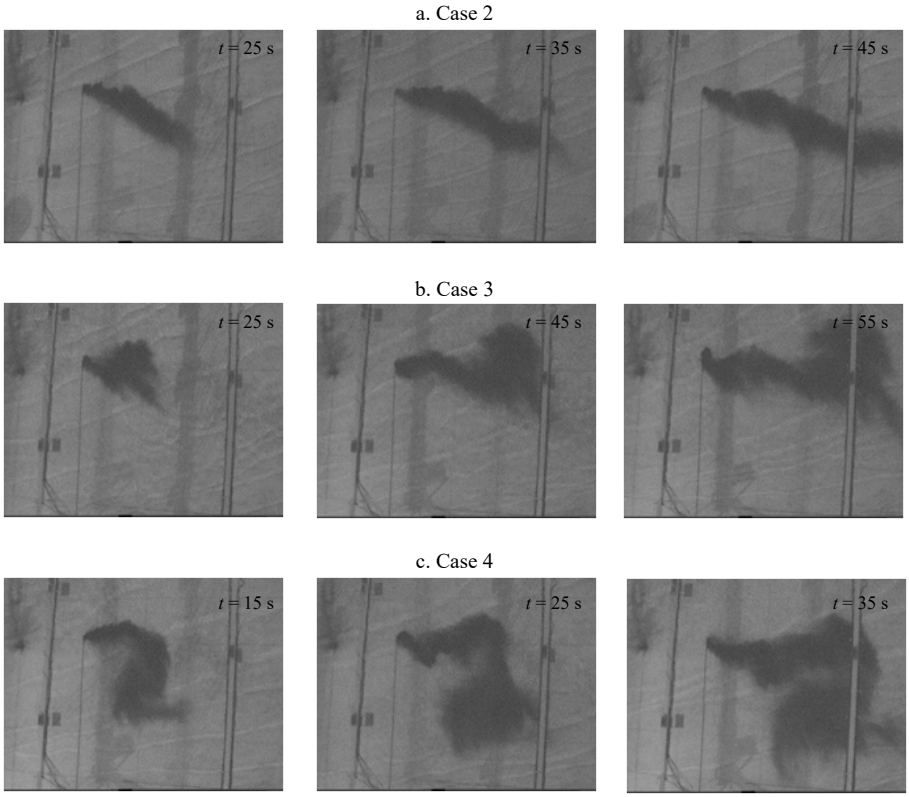

Fig. 8. Deformation of dye patch at three different times for Case 2 (a), Case 3 (b), and Case 4 (c).

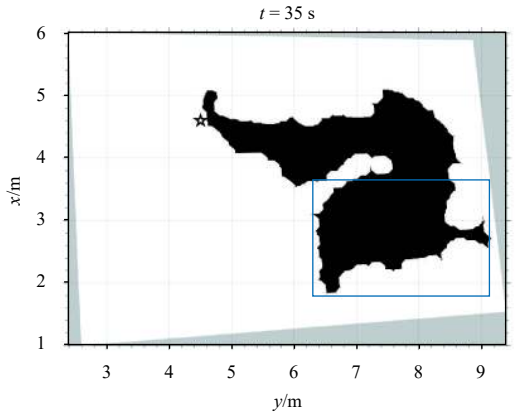

Fig. 9. Transformed dye patch at t = 35 s for Case 4. The blue rectangular box indicates the eddy dye patch.

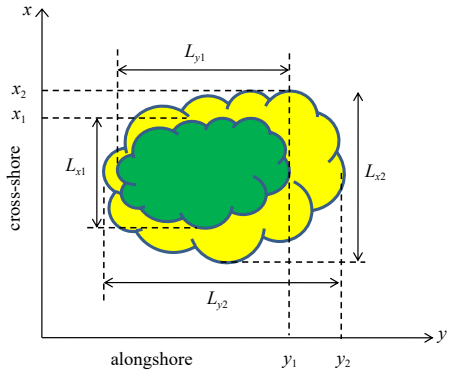

Fig. 10. Definition of length scale parameters for dye patch.

transported in the cross-shore direction. For Case 3, we observed that the eddy patches transported seaward took longer time. In other words, eddy patches did not form completely. The diffusion in the alongshore direction is dominated by longshore currents. Therefore, the weak diffusion alongshore for Case 2 (the value of wave height is the smallest) may be due to weak longshore currents. Another reason is that the present analysis was limited due to the fixed camera acquisition range; the environmental light was constantly changing. To some extent, it is essential to capturing the present images, particularly at the dye front, where the concentration was low. Therefore, the low correlation coefficients may be attributed to the mentioned causing factors.

The estimated diffusion (V_{Dx}, V_{Dy}) and transport velocity (V_{Tx}, V_{Ty}) for the selected four cases are summarized in Table 3. In the strong alongshore current, whether these eddy patches are of the same velocity with alongshore current velocity is still poorly understood, especially due to shear instability. Hence, the maximum mean alongshore current velocities (V_{max}) shown by Ren et al. (2012) for the four cases are also given in Table 3. Thus, we analyzed the characteristics of the eddy part by comparing V_{max} with V_{Dx}, V_{Dy}, V_{Tx}, and V_{Ty}.

We found that V_{Ty} is twice as large as V_{Tx}, indicating that alongshore currents are crucial in transporting eddy patches in the alongshore direction, even though surf zone eddies occur. Further, by comparing V_{Ty} with V_{max} under the same cases, V_{max} is approximately 1.1–2.6 times larger than V_{Ty}, indicating that the transport of eddy patches in the alongshore direction reduces due to the occurrence of surf zone eddies. In addition, V_{Dx} and V_{Dy} are in the range of 0.015–0.052 m/s, implying that the diffusion of eddy patches is weak relative to transport. Also, the extension magnitude is similar to previous study results (Clark et al., 2007, 2010).

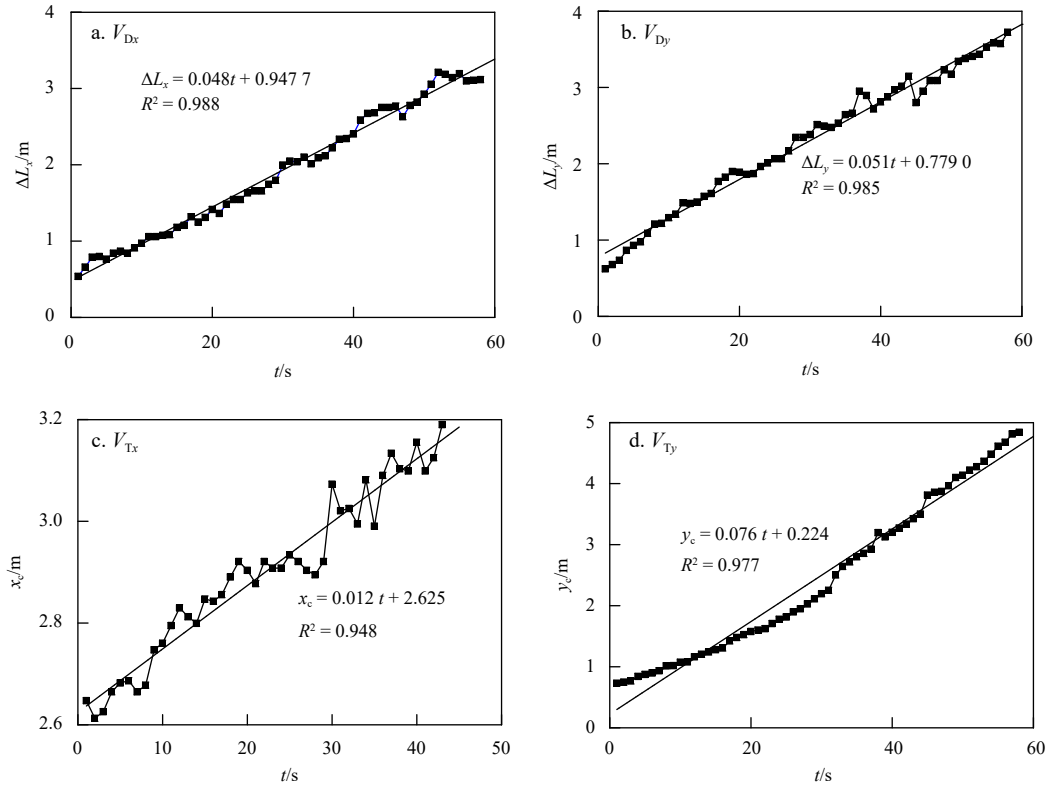

Fig. 11. Displacement of dye patch crest vs. time (diamond symbols) and its best-fit line (solid line) for Case 1. Wave condition-monochromatic regular waves with H = 2.7 cm and T = 1.5 s.

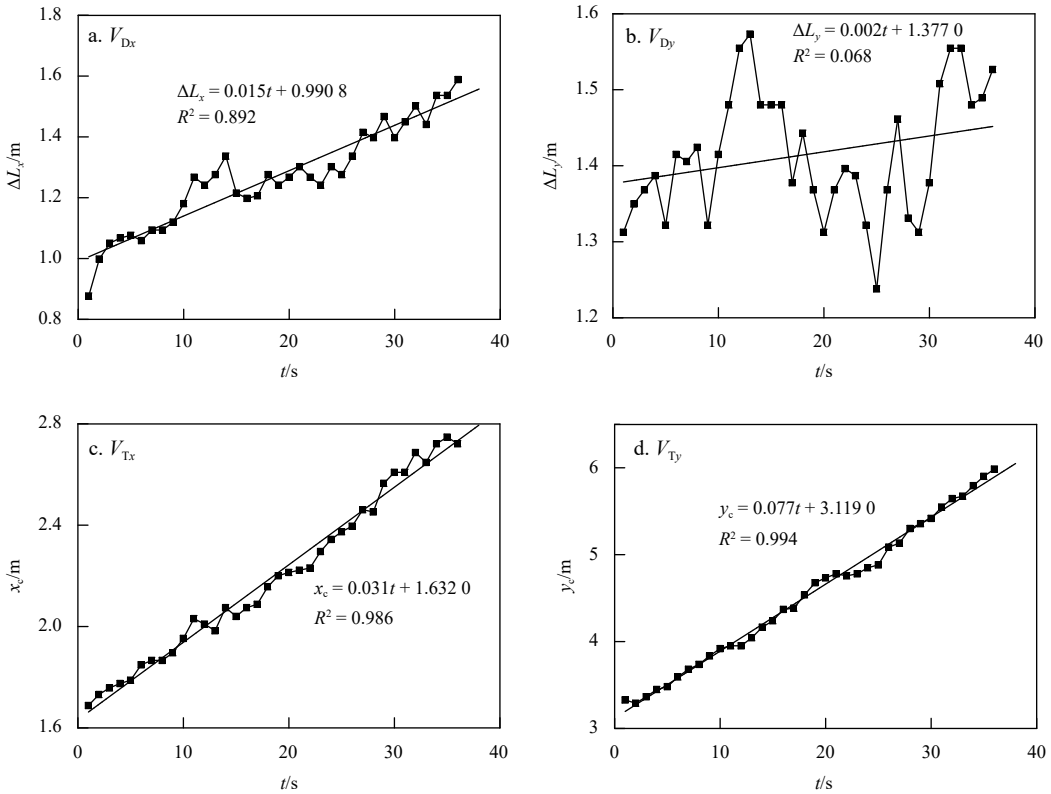

Fig. 12. Displacement of dye patch crest vs. time (diamond symbols) and its best-fit line (solid line) for Case 2 (wave condition-irregular waves with H = 2.4 cm and T = 1.0 s).

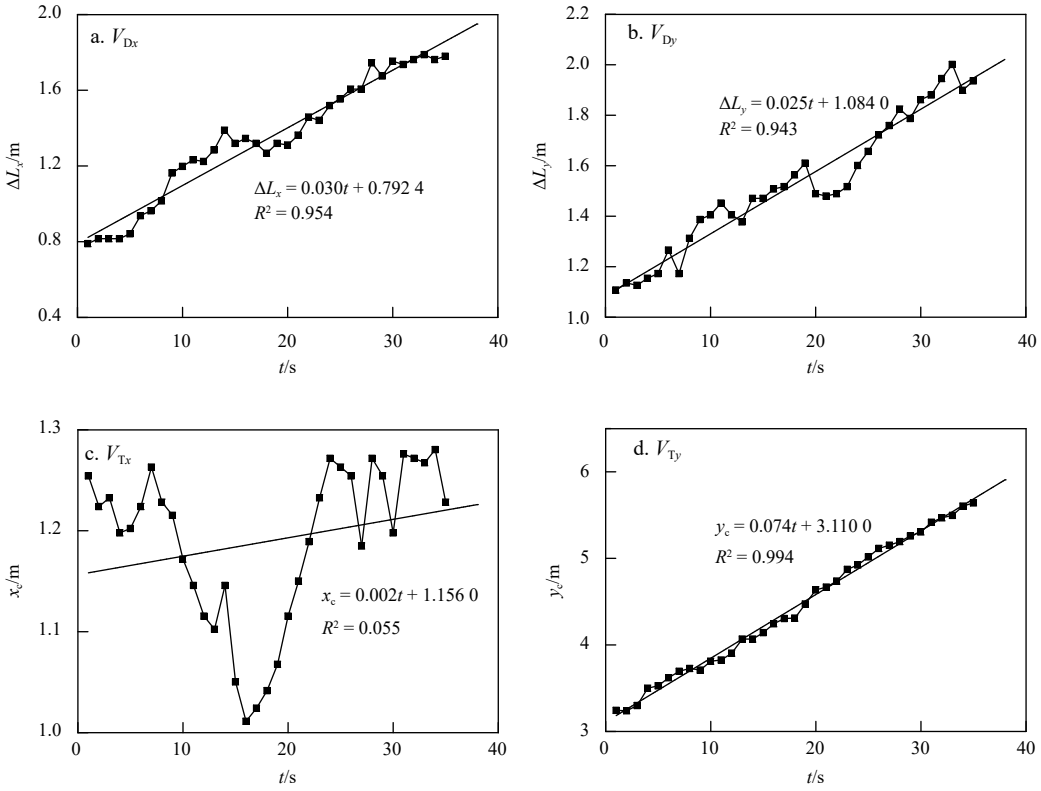

Fig. 13. Displacement of dye patch crest vs. time (diamond symbols) and its best-fit line (solid line) for Case 3 (wave condition-irregular waves with H = 3.9 cm and T = 1.0 s).

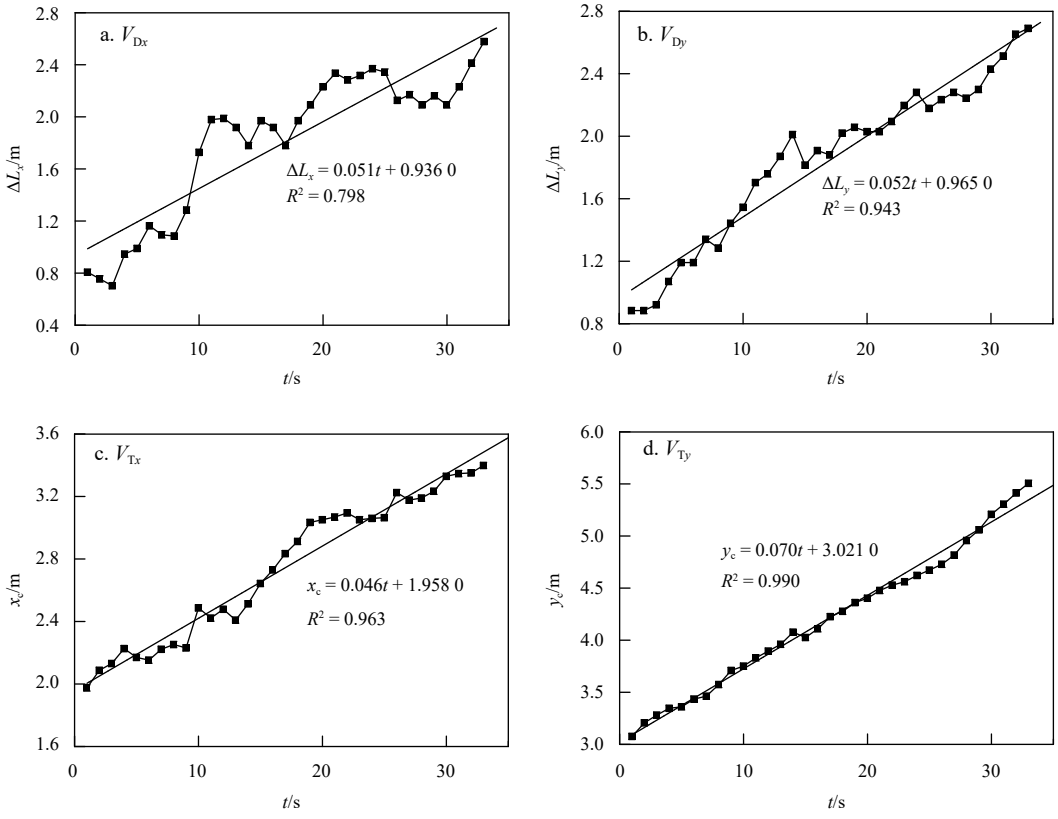

Fig. 14. Displacement of dye patch crest vs. time (diamond symbols) and its best-fit line (solid line) for Case 4 (wave condition-irregular waves with H = 5.0 cm and T = 1.5 s).

Table 3. Estimated extension and transport velocities of eddy patches for Cases 1–4

Case	V_{Dx}/(m · s^{-1})	V_{Dy}/(m · s^{-1})	V_{Tx}/(m · s^{-1})	V_{Ty}/(m · s^{-1})	V_{max}/(m · s^{-1})
1	0.048	0.051	0.012	0.076	0.16
2	0.015	*	0.031	0.077	0.10
3	0.030	0.025	*	0.074	0.14
4	0.051	0.052	0.046	0.070	0.19

Note: * denotes a very low coefficient of determination (R^2).

3.4 *Horizontal spatial scale*

The surf zone eddy shape patches occurred under Cases 1, 3, and 4, with an alongshore scale of approximately 2–4 m, 0.2–0.8 times the surf zone width; the cross-shore scale is roughly 1 m. The water depth was roughly 0.045 m at the dye release location. Therefore, the horizontal length scale was more significant than the water depth. These ratios of alongshore length scale to the surf zone width at the initial stage suggest that these present surf zone eddies are drastically different from those generated through the extrinsic mechanism of breaking wave vorticity forcing because they were formed at a smaller time scale. However, transient rips generated on alongshore uniform bathymetries are generally brief (2–5 min) and can migrate with an alongshore current (Castelle et al., 2016).

Moreover, according to the extrinsic mechanism, surf zone small-scale eddies due to wave breaking are hypothesized to coalesce and form larger eddies through nonlinear interactions, generating vortical motions in the surf zone over a wide range of spatial scales (Feddersen, 2014). Under similar incident wave conditions, numerical modeling demonstrated that vorticities of similar scales with the present occurred in the surf zone, and shear instability was crucial in generating these eddies. Section 4 presents the linear instability theory analysis performed to illustrate the horizontal length scales.

The analysis of the spatial scale of the surf zone eddy is hugely significant for validating the eddy generation mechanism. With the extrinsic mechanism, the small-scale eddies are hypothesized to coalesce and form larger eddies through nonlinear interactions, generating vortical motions in the surf zone over a wide range of spatial scales (from 10 m to 100 m) (Feddersen, 2014). However, according to linear instability theory, surf zone eddy can be generated more straight forwardly, agreeing with the present observation. There is a question about why the extrinsic mechanism can hardly explain the surf zone generation in a strong alongshore current. Further details are needed to explore in the future.

The 2D spatial scale of the surf zone eddy can be reflected straight with ΔL_x, ΔL_y (Eqs (1) and (2)) and compared with the width of the surf zone. Table 2 lists the width of the surf zone for four cases. Figure 14 depicts the $\Delta L_x/x_b$, $\Delta L_y/x_b$ variation over time. Overall, the evolution of the eddy patch scale can be divided into two stages: the first stage (Ⅰ) and the approximately stable stage (Ⅱ) (Fig. 15). For Cases 2–4 (irregular wave incidence), the duration in the first stage is approximately 30 s and 10 s in the cross-shore and alongshore directions, respectively. The eddy scale in both directions is roughly 0.1–0.2 times the width of the surf zone in the initial stage and larger than 0.2 in the stable stage. Case 1 is distinct from the other three cases; these eddies were more developed, and the horizontal scale can reach 0.5 times the width of the surf zone. The shoreline constrains the evolution of these eddies due to their occurrence on the shore side. If it occurs on the offshore side, it is possible to form larger-scale eddies. Through numerical studies, Chen et al. (2013) found that the surf zone eddy scale can reach 1.5 times the width of the surf zone.

4 Numerical analysis

4.1 *Shear instability theory model*

Shear instability theory was first developed to explain the meandering motions observed in fields at 10^{-3}–10^{-2} Hz frequencies and with wavelengths whose magnitude were too short to be gravity waves. Subsequently, shear instabilities of the mean alongshore current have been investigated based on a nonlinear shallow water equation with steady wave forcing (Allen et al., 1996; Noyes et al., 2005; Özkan-Haller and Kirby, 1999; Slinn et al., 1998). However, the effects of surf zone eddy induced by shear instability on dye transport patterns are poorly understood. Therefore, this section performs numerical analysis to validate whether the shear instability can induce perturbation velocity fields that may dominate the eddy patch deformation in the present strong alongshore current.

Shear instability theory has been described in detail elsewhere (Bowen and Holman, 1989; Dodd et al., 2004; Putrevu and Svendsen, 1992). Briefly, in a strong alongshore current, the uneven distribution of the time-average alongshore current $V(x)$ in the cross-shore direction results in the shear of the flow $\left(\frac{\partial V}{\partial x}, \frac{\partial^2 V}{\partial x^2}\right)$, persistently driving far infragravity motions. The maximum growth mode is assumed to dominate the time and length scale and perturbation velocity field patterns. Shear instability theory was developed assuming that the flow velocity field is represented by a steady longshore current $V(x)$ with small superimposed perturbations $\boldsymbol{u}'(x, y, t) = (u'(x, y, t),$

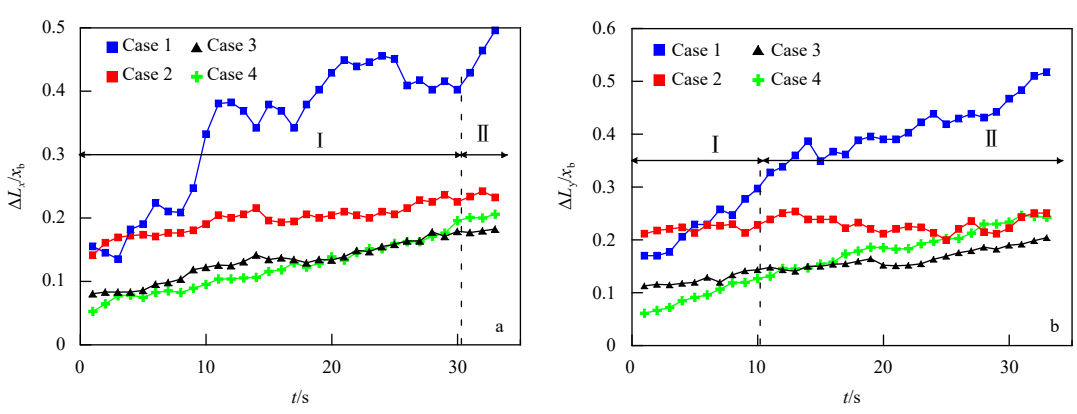

Fig. 15. Variations in the ratios of the cross-shore (a) and alongshore (b) eddy scale to x_b with time.

$v'(x, y, t)\big)$ as follows:

$$\boldsymbol{u}(x, y, t) = \big(u'(x, y, t), V(x) + v'(x, y, t)\big), \tag{5}$$

where x and y are horizontal two-dimensional coordinates; the x axis is perpendicular to the shoreline and positive offshore from the shoreline; the y axis is the alongshore coordinate; $\boldsymbol{u}$ is the depth-averaged current velocity; t is time.

The shallow water, inviscid equations for horizontal momentum are as follows:

$$\nabla \cdot (h\boldsymbol{u}) = 0, \tag{6}$$

$$\boldsymbol{u}_t + (\boldsymbol{u} \cdot \nabla)\boldsymbol{u} + g\nabla\eta = 0, \tag{7}$$

where $\nabla = (\partial/\partial x, \partial/\partial y)$; η is the average sea surface elevation; h is the water depth; g is the gravitational acceleration.

$\boldsymbol{u}$ is represented in terms of a stream function ψ. Furthermore, the perturbation may be assumed as follows:

$$u' = -\frac{\psi_y}{h} = -\frac{\mathrm{i}\varphi k}{h}\exp(\omega_\mathrm{i} t)\exp[\mathrm{i}(ky - \omega_\mathrm{r} t)], \tag{8}$$

$$v' = \frac{\psi_x}{h} = \frac{\varphi_x}{h}\exp(\omega_\mathrm{i} t)\exp[\mathrm{i}(ky - \omega_\mathrm{r} t)], \tag{9}$$

where $\psi(x, y, t)$ is the stream function, $\varphi(x)$ is the amplitude, ω_r is the angular frequency, ω_i is the growth rate; $\omega = \omega_\mathrm{r} + \mathrm{i}\omega_\mathrm{i}$, k is the wave number; and i is the imaginary unit. Then, substituting Eqs (5), (8), and (9) into the two-dimensional shallow water Eqs (6) and (7) under the assumption of "rigid lid", the following equation governing the instability is derived.

$$(V - c)\left(\varphi_{xx} - k^2\varphi - \frac{\varphi_x h_x}{h}\right) - h\varphi\left(\frac{V_x}{h}\right)_x = 0, \tag{10}$$

where V is the mean alongshore current, $c = \omega/k = c_\mathrm{r} + \mathrm{i}c_\mathrm{i}$. The solid curves fitted to the results (Fig. 6) were used as input data for the linear instability analysis.

4.2 *Theoretical calculation results of the instability mode*

For a given water depth $h(x)$, mean velocity profile $V(x)$, and wavenumber k solving Eq. (10) gives N eigenvalues of c and eigenfunction $\varphi(x)$. The case $\omega_\mathrm{i} > 0$ shows the shear instabilities of longshore currents; otherwise, longshore currents are stable. Of N eigenvalues of c, it is assumed that the eigenvalue with the largest imaginary component dominates the instability of that wavenumber. Here, we take this largest imaginary component as the final solution for c in Eq. (10).

The velocity profile of the mean longshore currents (fitted results) for Cases 1–4 (Fig. 6) was adopted as the background shear flows in the linear instability analysis, with the fitted lines in place of the discrete test data. Figure 16 shows the growth rate, ω_i (Fig. 16a), and the propagation speed, c_r (Fig. 16b) of the shear waves vs. wave number k for Cases 1–4. We observed two peaks for all cases. The first peak corresponds to the backshear mode (red up-arrow for Case 1 in Fig. 16a), and the second corresponds to the frontshear mode (black up-arrow for Case 1). However, the second mode for Case 1 corresponds to stronger growth rate than the first mode, entirely different for Cases 1–3. It demonstrated that frontshear had much more significant effects on the instabilities for Case 1.

For Cases 1–4, the wave number (k_0) and the propagation speed (c_r), period ($T = 2\pi/(k_0 c_\mathrm{r})$ and wavelength ($L = 2\pi/k_0$) of the shear waves corresponding to the two modes are given in Table 4. It is suggested that the calculated wavelength corresponding to the frontshear mode agrees with the observed horizontal dye patch scales, suggesting a frontshear mode for the ob-

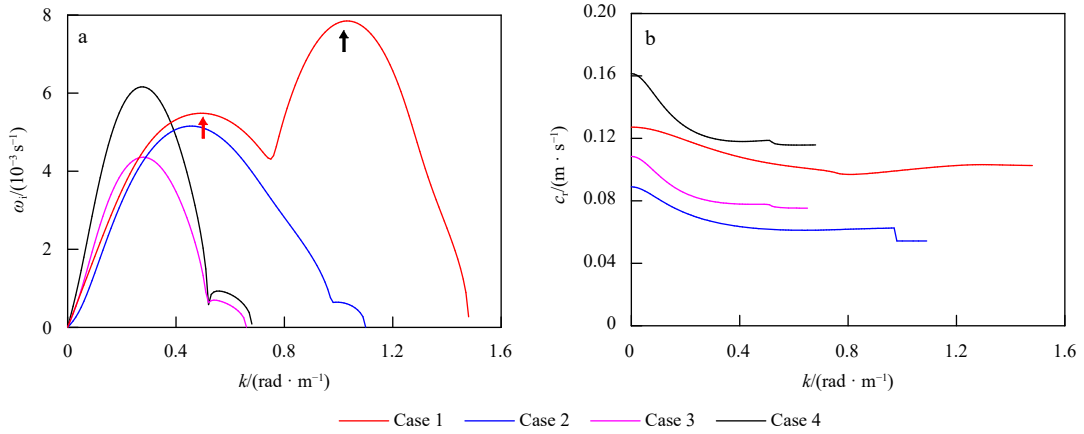

Fig. 16. Variations of growth rate (ω_i, a) and propagation speed (c_r, b) vs. wavenumber (k) for Cases 1–4. The red arrow and black arrow denote the first mode and second mode, respectively.

Table 4. Numerical results of shear waves for Cases 1–4

Case	$k_{0,1}$	$c_{\mathrm{r},1}$	T_1	L_1	$k_{0,2}$	$c_{\mathrm{r},2}$	T_2	L_2
	First mode				Second mode			
1	0.490	0.105	122.41	12.82	1.030	0.100	60.93	6.10
2	0.460	0.062	218.92	13.65	0.990	0.054	116.88	6.34
3	0.280	0.080	279.48	22.43	0.620	0.076	133.28	10.13
4	0.280	0.121	185.48	22.43	0.560	0.116	96.72	11.21

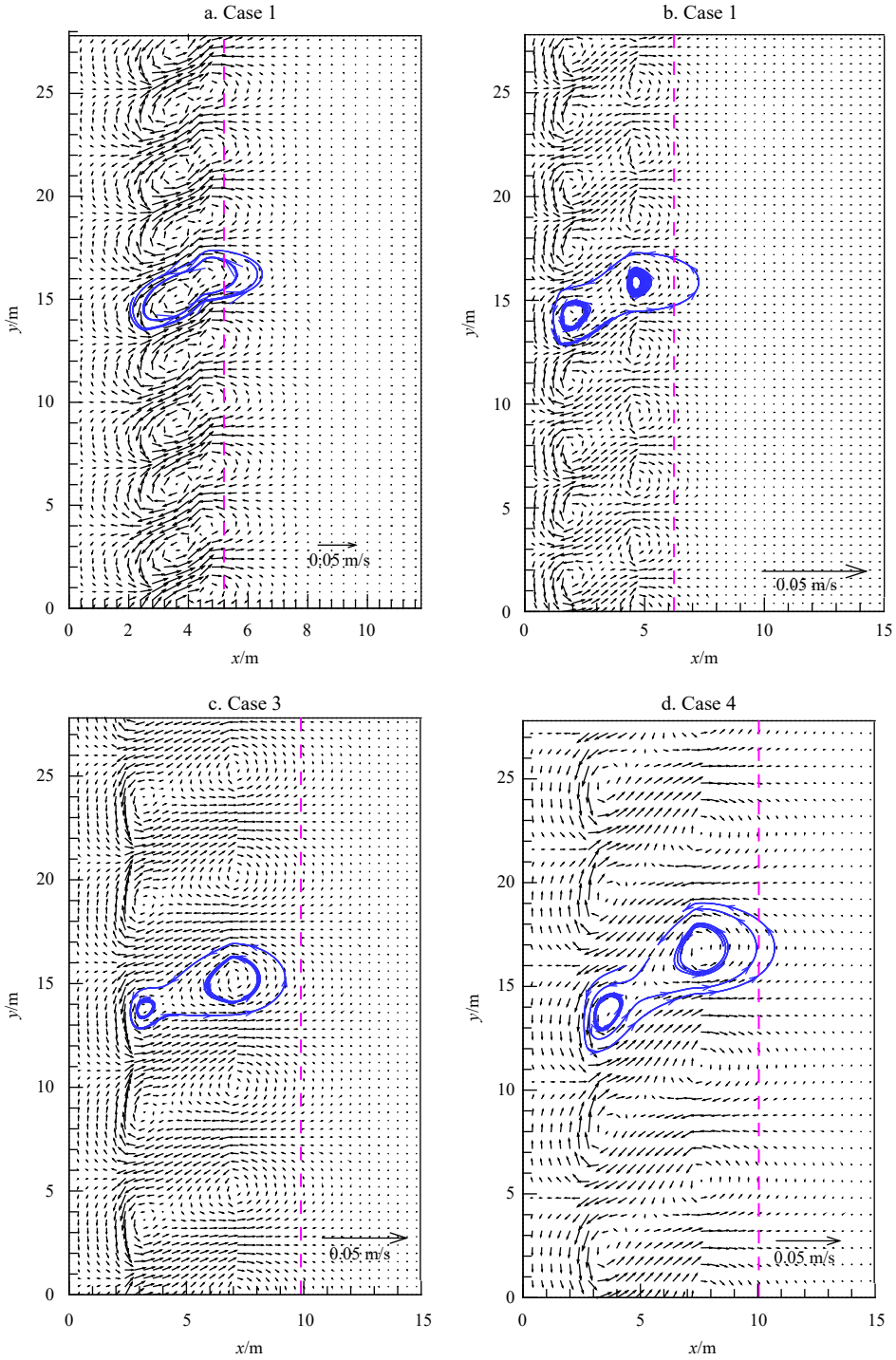

Fig. 17. Calculated perturbation velocity fields for Cases 1–4. The blue streamlines show the vortex velocity; the red dashed line shows the location of the wave breaking.

served shear waves under the present four wave conditions.

4.3 *Perturbation velocity field*

According to this analysis, the perturbation velocity field $u'(x, y, t) = \left(u'(x, y, t), v'(x, y, t)\right)$, corresponding to the second mode, can be calculated using to Eqs (8)–(10). Figure 17 illustrates the corresponding disturbance velocity fields at the initial time of the four cases and the location of the wave breaking (red dashed line). The vortex velocity fields occur periodically alongshore with a scale similar to the observed eddy patches in the experiment in the surf zone. The magnitude of disturbance velocity (0.05 m/s) is close to the alongshore transport velocity of eddy patches (0.07 m/s) estimated in Section 3.3. Also, the disturbance velocity field is approximately a single vortex pattern for Case 1 (regular wave incidence). However, a double vortex field occurs for Cases 2–4 (irregular wave incidence), as indicated by a blue streamline. It may be attributed to different alongshore current velocity profiles (or different alongshore current shears) in the cross-shore direction induced by different incident waves. Under irregular incident wave conditions, it is easier to induce an

eddy field with a more complex structure owing to the larger backshear (the inflection point occurs at the back side (seaward side) of the velocity profile) (Baquerizo et al., 2001). The collected dye patches under test conditions 2–4, mainly generated in the wave-breaking zone, can validate this phenomenon, presenting a meandering pattern or ejecting onshore or offshore. It can be attributed to the structure of the double vortex velocity field. More importantly, the horizontal length scales of surf zone eddy patches are approximately consistent with the numerically calculated vortex. Therefore, this numerical analysis suggests that the linear instability theory can correctly explain the transport evolution of observed eddy patches dominated by surf zone eddies in the strong alongshore current.

5 Discussion

The experimental measurement duration in this study was short, and the collecting range of dye patch movement was smaller than the field scale. Compared with the field test with long distance and long measurement time, other factors (such as wind, temperature, tide, etc.) (Kumar and Feddersen, 2017a, b) cannot be considered. On the other hand, image collecting and proceeding may bring errors in estimating the transport and diffusion due to experimental light and treatment technology of determining surf zone eddy patch boundary. In addition, while the results suggest the dominant plume behaviors are explained well by shear instability theory, aspects of the surf zone plume behavior may vary due to interaction with shelf processes, including Stokes drift, internal waves, fronts, and adjacent plumes.

The solid curves fitted to the results (Fig. 6) were used as input data for the linear instability analysis. However, the mean longshore current's velocity profile significantly affected the instability mode (Ren et al., 2012). Also, different fitting methods may result in differences among these calculated perturbation velocity fields. They can be ignored due to the dominance of backshear to the shear instability mode. In other words, selected fitting methods have negligible effects on the backshear. Since the mean alongshore currents are regarded as being steady, only the calculated perturbation velocity fields are at the initial time given. However, nonlinear numerical modeling has demonstrated that the mixing induced by shear instability may adjust the velocity profile of the mean longshore current with time (Özkan-Haller and Kirby, 1999). Therefore, in the future, related numerical analysis should be conducted to investigate the time-dependent evolution of perturbation velocity induced by shear instability. In addition, numerical modeling with a phase-resolving Boussinesq-type wave model (such as funwaveC) (Feddersen et al., 2011) and a comparison between numerical and experimental results should be performed to diagnose the effect of shear instability with a strong current on dye patch transport in the surfzone. Such studies would allow for a more detailed understanding of the surf zone generation mechanism and address whether the surf zone eddy is dominated by shear instability rather than the breaking wave vorticity forcing or partly in a strong alongshore current.

6 Conclusions

In this paper, the evolution, propagation, and diffusion characteristics of surf zone eddies generated by shear instabilities were analyzed by dye patch tracing experiments. Also, the surf zone eddies generation mechanism was analyzed based on shear instability theory. The results demonstrated that under monochromatic unidirectional incident waves with a large angle of incidence, the surf zone eddies were generated in the shoreward and offshore directions on a plane beach. The eddy patches' alongshore and cross-shore scale was approximately 4 m and 1 m, respectively.

We found that visible eddy or alongshore meandering patches occurred for the four test cases during the evolution of dye patches. These eddy patches were mainly transported in the alongshore direction. The alongshore propagation speed was approximately twice that of the cross-shore, and the cross-shore and alongshore diffusion speeds were weak (approximately 0.05 m/s). The development of these eddy patches can be roughly divided into two stages: in the initial stage, the eddy scale in both directions was about 0.1–0.2 times the width of the surf zone; in the stabilization stage, it was less than 0.2 times.

Based on shear instability theory, the perturbation velocity fields were obtained under the four wave conditions, showing that the velocity field structure was approximately consistent with the experimental observation. In addition, these velocity fields were more likely induced under random incident waves, which may drive double eddy. Consequently, the numerical analysis demonstrated that the linear instability theory could explain the transport evolution of observed eddy patches dominated by surf zone eddies in the strong alongshore current (Bowen and Holman, 1989; Brivois et al., 2012).

References

Abolfathi S, Cook S, Yeganeh-Bakhtiary A, et al. 2020. Microplastics transport and mixing mechanisms in the nearshore region. In: Lynett P J, ed. Proceedings of virtual Conference on Coastal Engineering, (36v): papers. 63, doi: 10.9753/icce.v36v.papers.63, https://icce-ojs-tamu.tdl.org/icce/article/view/10331 [2020-12-31/2023-05-01]

Abolfathi S, Pearson J. 2014. Solute dispersion in the nearshore due to oblique waves. In: Lynett P J, ed. Proceedings of 34th Conference on Coastal Engineering, (34): waves. 49, doi: 10.9753/icce.v34.waves.49, https://icce-ojs-tamu.tdl.org/icce/article/view/7803 [2014-10-30/2023-05-01]

Abolfathi S, Pearson J, 2017. Application of smoothed particle hydrodynamics (SPH) in nearshore mixing: a comparison to laboratory data. In: Lynett P J, ed. Proceedings of 35th Conference on Coastal Engineering, (35): currents. 16, doi: 10.9753/icce.v35.currents.16, https://icce-ojs-tamu.tdl.org/icce/article/view/8228 [2017-06-23/2023-05-01]

Allen J S, Newberger P A, Holman R A. 1996. Nonlinear shear instabilities of alongshore currents on plane beaches. Journal of Fluid Mechanics, 310: 181–213, doi: 10.1017/S0022112096001772

Baquerizo A, Caballeria M, Losada M A, et al. 2001. Frontshear and backshear instabilities of the mean longshore current. Journal of Geophysical Research: Oceans, 106(C8): 16997–17011, doi: 10.1029/2001JC900004

Bowen A J, Holman R A. 1989. Shear instabilities of the mean longshore current: 1. Theory. Journal of Geophysical Research: Oceans, 94(C12): 18023–18030, doi: 10.1029/JC094iC12p18023

Brivois O, Idier D, Thiébot J, et al. 2012. On the use of linear stability model to characterize the morphological behaviour of a double bar system. Application to Truc Vert Beach (France). Comptes Rendus Geoscience, 344(5): 277–287, doi: 10.1016/j.crte.2012.02.004

Brown J A, MacMahan J H, Reniers A J H M, et al. 2015. Field observations of surf zone-inner shelf exchange on a rip-channeled beach. Journal of Physical Oceanography, 45(9): 2339–2355, doi: 10.1175/JPO-D-14-0118.1

Castelle B, Scott T, Brander R W, et al. 2016. Rip current types, circulation and hazard. Earth-Science Reviews, 163: 1–21, doi: 10.1016/j.earscirev.2016.09.008

Clark D B, Feddersen F, Guza R T. 2010. Cross-shore surfzone tracer dispersion in an alongshore current. Journal of Geophysical Re-

search: Oceans, 115(C10): C10035, doi: 10.1029/2009JC005683
Clark D B, Feddersen F, Guza R T. 2011. Modeling surf zone tracer plumes: 2. Transport and dispersion. Journal of Geophysical Research: Oceans, 116(C11): C11028, doi: 10.1029/2011JC007211
Clarke L B, Ackerman D, Largier J. 2007. Dye dispersion in the surf zone: measurements and simple models. Continental Shelf Research, 27(5): 650–669, doi: 10.1016/j.csr.2006.10.010
Dodd N, Iranzo V, Caballeria M. 2004. A subcritical instability of wave-driven alongshore currents. Journal of Geophysical Research: Oceans, 109(C2): C02018, doi: 10.1029/2001JC001106
Feddersen F. 1998. Weakly nonlinear shear waves. Journal of Fluid Mechanics, 372: 71–91, doi: 10.1017/S0022112098002158
Feddersen F. 2012. Scaling surf zone turbulence. Geophysical Research Letters, 39(18): L18613, doi: 10.1029/2012GL052970
Feddersen F. 2014. The generation of surfzone eddies in a strong alongshore current. Journal of Physical Oceanography, 44(2): 600–617, doi: 10.1175/JPO-D-13-051.1
Feddersen F, Clark D B, Guza R T. 2011. Modeling surf zone tracer plumes: 1. Waves, mean currents, and low-frequency eddies. Journal of Geophysical Research: Oceans, 116(C11): C11027, doi: 10.1029/2011JC007210
Grimes D J, Feddersen F, Giddings S N, et al. 2020a. Cross-shore deformation of a surfzone-released dye plume by an internal tide on the inner shelf. Journal of Physical Oceanography, 50(1): 35–54, doi: 10.1175/JPO-D-19-0046.1
Grimes D J, Feddersen F, Giddings S N. 2021. Long-distance/time surf-zone tracer evolution affected by inner-shelf tracer retention and recirculation. Journal of Geophysical Research: Oceans, 126(12): e2021JC017661, doi: 10.1029/2021JC017661
Grimes D J, Feddersen F, Kumar N. 2020b. Tracer exchange across the stratified inner-shelf driven by transient rip-currents and diurnal surface heat fluxes. Geophysical Research Letters, 47(10): e2019GL086501, doi: 10.1029/2019GL086501
Hally-Rosendahl K, Feddersen F. 2016. Modeling surfzone to inner-shelf tracer exchange. Journal of Geophysical Research: Oceans, 121(6): 4007–4025, doi: 10.1002/2015JC011530
Hally-Rosendahl K, Feddersen F, Clark D B, et al. 2015. Surfzone to inner-shelf exchange estimated from dye tracer balances. Journal of Geophysical Research: Oceans, 120(9): 6289–6308, doi: 10.1002/2015JC010844
Hally-Rosendahl K, Feddersen F, Guza R T. 2014. Cross-shore tracer exchange between the surfzone and inner-shelf. Journal of Geophysical Research: Oceans, 119(7): 4367–4388, doi: 10.1002/2013JC009722
Holland T K, Holman R A, Lippmann T C, et al. 1997. Practical use of video imagery in nearshore oceanographic field studies. IEEE Journal of Oceanic Engineering, 22(1): 81–92, doi: 10.1109/48.557542
Johnson D, Pattiaratchi C. 2004. Application, modelling and validation of surfzone drifters. Coastal Engineering, 51(5/6): 455–471, doi: 10.1016/j.coastaleng.2004.05.005
Kumar N, Feddersen F. 2017a. The effect of Stokes drift and transient rip currents on the inner shelf. Part I: no stratification. Journal of Physical Oceanography, 47(1): 227–241, doi: 10.1175/JPO-D-16-0076.1
Kumar N, Feddersen F. 2017b. The effect of stokes drift and transient rip currents on the inner shelf. Part II: with stratification. Journal of Physical Oceanography, 47(1): 243–260, doi: 10.1175/JPO-D-16-0077.1
Long J W, Özkan-Haller H T. 2009. Low-frequency characteristics of wave group–forced vortices. Journal of Geophysical Research: Oceans, 114(C8): C08004, doi: 10.1029/2008JC004894
Longuet-Higgins M S. 1970. Longshore currents generated by obliquely incident sea waves: 2. Journal of Geophysical Research, 75(33): 6790–6801, doi: 10.1029/JC075i033p06790
Moulton M, Chickadel C C, Thomson J. 2021. Warm and cool nearshore plumes connecting the surf zone to the inner shelf. Geophysical Research Letters, 48(10): e2020GL091675, doi: 10.1029/2020GL091675
Noyes T J, Guza R T, Elgar S, et al. 2004. Field observations of shear waves in the surf zone. Journal of Geophysical Research: Oceans, 109(C1): C01031, doi: 10.1029/2002JC001761
Noyes T J, Guza R T, Feddersen F, et al. 2005. Model-data comparisons of shear waves in the nearshore. Journal of Geophysical Research: Oceans, 110(C5): C05019, doi: 10.1029/2004JC002541
O'Dea A, Kumar N, Haller M C. 2021. Simulations of the surf zone eddy field and cross-shore exchange on a nonidealized bathymetry. Journal of Geophysical Research: Oceans, 126(5): e2020JC016619, doi: 10.1029/2020JC016619
Oltman-Shay J, Howd P A, Birkemeier W A. 1989. Shear instabilities of the mean longshore current: 2. field observations. Journal of Geophysical Research: Oceans, 94(C12): 18031–18042, doi: 10.1029/JC094iC12p18031
Özkan-Haller H T, Kirby J T. 1999. Nonlinear evolution of shear instabilities of the longshore current: a comparison of observations and computations. Journal of Geophysical Research: Oceans, 104(C11): 25953–25984, doi: 10.1029/1999JC900104
Pearson J M, Guymer I, West J R, et al. 2009. Solute mixing in the surf zone. Journal of Waterway, Port, Coastal, and Ocean Engineering, 135(4): 127–134, doi: 10.1061/(ASCE)0733-950X(2009)135:4(127)
Peregrine D H. 1998. Surf zone currents. Theoretical and Computational Fluid Dynamics, 10(1–4): 295–309, doi: 10.1007/s001620050065
Putrevu U, Svendsen I A. 1992. Shear instability of longshore currents: a numerical study. Journal of Geophysical Research: Oceans, 97(C5): 7283–7303, doi: 10.1029/91JC02988
Ren Chunping, Zou Zhili, Qiu Dahong. 2012. Experimental study of the instabilities of alongshore currents on plane beaches. Coastal Engineering, 59(1): 72–89, doi: 10.1016/j.coastaleng.2011.07.004
Reniers A J H M, Battjes J A. 1997. A laboratory study of longshore currents over barred and non-barred beaches. Coastal Engineering, 30(1/2): 1–21, doi: 10.1016/S0378-3839(96)00033-6
Reniers A J H M, Battjes J A, Falqués A, et al. 1997. A laboratory study on the shear instability of longshore currents. Journal of Geophysical Research: Oceans, 102(C4): 8597–8609, doi: 10.1029/96JC03863
Reniers A J H M, Thornton E B, Stanton T P, et al. 2004. Vertical flow structure during Sandy Duck: observations and modeling. Coastal Engineering, 51(3): 237–260, doi: 10.1016/j.coastaleng.2004.02.001
Slinn D N, Allen J S, Newberger P A, et al. 1998. Nonlinear shear instabilities of alongshore currents over barred beaches. Journal of Geophysical Research: Oceans, 103(C9): 18357–18379, doi: 10.1029/98JC01111
Spydell M S. 2016. The suppression of surfzone cross-shore mixing by alongshore currents. Geophysical Research Letters, 43(18): 9781–9790, doi: 10.1002/2016GL070626
Spydell M S, Feddersen F. 2012a. A Lagrangian stochastic model of surf zone drifter dispersion. Journal of Geophysical Research: Oceans, 117(C3): C03041, doi: 10.1029/2011JC007701
Spydell M S, Feddersen F. 2012b. The effect of a non-zero Lagrangian time scale on bounded shear dispersion. Journal of Fluid Mechanics, 691: 69–94, doi: 10.1017/jfm.2011.443
Tang Jun, Lyu Yigang, Shen Yongming. 2016. Numerical simulation of the Kuroshio intrusion into the South China Sea by a passive tracer. Acta Oceanologica Sinica, 35(9): 111–116, doi: 10.1007/s13131-016-0932-8
Visser P J. 1991. Laboratory measurements of uniform longshore currents. Coastal Engineering, 15(5/6): 563–593, doi: 10.1016/0378-3839(91)90028-F
Wu Xiaodong, Feddersen F, Giddings S N, et al. 2020. Mechanisms of mid-to outer-shelf transport of shoreline-released tracers. Journal of Physical Oceanography, 50(7): 1813–1837, doi: 10.1175/JPO-D-19-0225.1